Received 11 January 2024; revised 2 February 2024; accepted 11 February 2024. Date of publication 19 February 2024; date of current version 4 March 2024.

Digital Object Identifier 10.1109/OJCOMS.2024.3367457

Aqua-Sense: Relay-Based Underwater Optical Wireless Communication for IoUT Monitoring

MAAZ SALMAN[1], JAVAD BOLBOLI[1], RAMAVATH PRASAD NAIK[2] (Member, IEEE), AND WAN-YOUNG CHUNG[1] (Senior Member, IEEE)

[1]Department of Artificial Intelligence and Convergence, Pukyong National University, Busan 48513, Republic of Korea

[2]Department of Electronics and Communication Engineering, National Institute of Technology Rourkela, Rourkela 769008, India

CORRESPONDING AUTHOR: W.-Y. CHUNG (e-mail: chung.wanyoung@gmail.com)

This work was supported by the National Research Foundation of Korea (NRF) Grant funded by the Korea Government (MIST) under Grant NRF-2019R1A2C1089139.

ABSTRACT Underwater wireless optical communication (UWOC) performance is negatively impacted by challenges such as water turbulence, restricted range, and misalignment. These challenges can impact the feasibility of large-scale deployment. In comparison to conventional acoustic and radio frequency (RF) communication, UWOC can play a pivotal role in connecting various Internet of Underwater Things (IoUT) devices. This research presents the design and evaluation of "aqua-sense," a relay-based UWOC system aimed at enhancing communication link performance and expanding the reception area of the optical receiver. To harness diversity gain, the optical relay incorporates combining techniques such as Equal Gain Combining (EGC), Majority Logic Combining (MLC), and Selection Combining (SC) to enhance its performance. Additionally, the optical relay, referred to as the "opto-relay," is empowered by a channel-aware algorithm to further improve communication link performance. In moderately turbid water conditions with a turbidity level of 25 NTU, the aqua-sense system achieved a packet success rate of 68% at a communication link distance of up to 7.5 meters, transmitting at a rate of 0.2 Mbps. Additionally, the sensor node, "opto-sense," achieved a consistent transmission rate of 0.5 Mbps in clear water with a turbidity of 0.01 NTU. These results remained stable even when moderate water waves with a displacement rate of 5 liters/min and air bubbles with an airflow rate of 5 liters/min were present within a 2-meter communication link range.

INDEX TERMS Relay-based UWOC, aqua-sense, packet success rate, bit error rate.

I. INTRODUCTION

WIRELESS communication is vital for a wide range of applications, both indoors and outdoors, enabling connectivity among numerous Internet of Things (IoT) devices [3]. This has sparked a transformative wave in IoT device interconnectivity, serving purposes such as data collection and a multitude of other applications. These applications are designed to provide real-time environmental insights through robust communication [4]. However, a significant portion of underwater regions, including sub-sea habitats, remain unexplored due to the lack of affordable communication components suitable for the challenging underwater conditions. The advancement in underwater wireless communication can yield benefits in various applications, including predicting volcanic activities through seafloor temperature monitoring, assessing the health and tracking the location of marine habitats using inertial moment sensors, and monitoring underwater pollution [5], [6], [7], [8]. Currently, existing underwater sensor networks rely heavily on manual operations or complex and expensive underwater vehicles and instruments. This reliance introduces numerous operational challenges:

1) Sensor deployment, retrieval, and real-time usage entail laborious and cumbersome processes.
2) Manual management of the sensor network diminishes efficiency and increases the likelihood of errors.

© 2024 The Authors. This work is licensed under a Creative Commons Attribution-NonCommercial-NoDerivatives 4.0 License.
For more information, see https://creativecommons.org/licenses/by-nc-nd/4.0/

3) The positioning and installation of sensors introduce delays in obtaining valuable data, constraining their usefulness and reliability in time-sensitive applications.
4) Individual sensor operations are confined to a limited spatial area for data collection.
5) The absence of interconnectivity among sensors leads to the breakdown of functions that necessitate collaboration between sensor nodes, such as event localization and tracking various movements.

To address these challenges, the concept of IoUT is proposed such as offshore aquaculture, mapping, underwater modelling, and monitoring of marine biology and ocean floor [14]. The concept of an underwater wireless sensor network (UWSN) has been proposed to mimic the full potential of IoT in underwater environments [15]. In principle, the UWSN integrates communication, computation, supporting algorithms, and sensing capabilities. For non-intrusive, real-time monitoring applications, wireless communication is critical. As such, the ability of in situ data transmission is the most critical aspect for underwater observatory [16]. A sensor node is a primary component of the UWSN, comprising a communication modem, battery, and sensors. The predominant method is acoustic communication, boasting communication ranges of up to tens of miles with a low bit-error rate [9]. However, acoustic signals are prone to the stochastic nature of the underwater environment, leading to multi-path propagation. Consequently, it suffers from notable drawbacks, including high latency, limited bandwidth, and multi-path propagation [7], [10]. Radio technologies provide an alternate option, although they are limited by a communication range of only a few meters [11], [51]. These limitations have prompted the consideration and adoption of UWOC, which offers minimal latency, high data rates, and a moderate communication range [12]. Moreover, UWOC provides a wide unregulated frequency spectrum (400–800 THz), low latency, and high data rate [19]. Furthermore, the UWOC consumes significantly less power compared to acoustic communication owing to the utilization of fewer complex components and processing [7], which is paramount for small mobile platforms (SMP) applications. An early underwater analogue communication system is reported in [17], which monitors the neuronal activity of crayfish and transmits the information to the corresponding gateway. For sea floor monitoring and observatories, an early prototype of an optical wireless communication system has been designed and evaluated in [18].

More recent and past works are focused on complex solutions to gain high bandwidth for robust and reliable communication. To achieve these desired objectives for the development of a system prototype, complex and bulky modules are required. In [24], [25], [26], the authors performed experiments with a laser source over a 5 m distance to transfer real-time high-volume data. An acoustic-optical hybrid network for mobile sensors is suggested in [27]. In [28], commercial blue LEDs were used to transmit real-time picture data, and in [29], vertical communication was tested to monitor IoT systems in oil rigs. Although UWOC promises potential communication credentials, it encounters certain challenges, such as limited range (tens of meters), path loss, loss of data due to beam misalignment, and the critical requirement of line-of-sight communication [20]. Although the highlighted studies have shed conclusive light and laid the experimental and theoretical foundations, the majority of the work is focused on theoretical evaluation and one-hop transmission. Furthermore, these systems have exploited complex, expensive, and bulky components to achieve high data rates and long ranges. In order to overcome the limitations of UWOC, such as restricted range, line of sight communication, and alignment issues, relaying and routing procedures can be employed to expand the range of communication [30], [31]. To this end, relay-assisted UWOC (RA-UWOC) can be used to mitigate these challenges, and accordingly, relay-based UWSNs have been proposed to improve the range and data transmission [19]. The graphical presentation of the proposed relay-based UWOC system is illustrated in Figure 1.

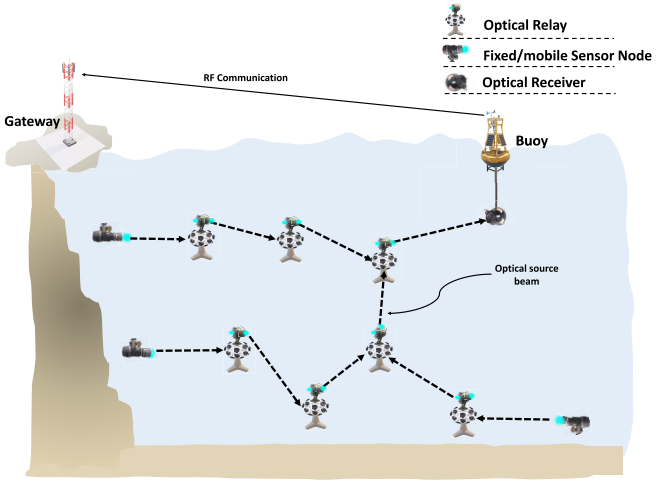

FIGURE 1. Scenario of relay-based UWOC system for UIoT monitoring.

II. RELATED WORKS AND AQUA-SENSE

In [37], [38], the authors investigated the viability of relay based UWOC and a three-hop underwater wireless acoustic communication (3H-UWAC) structure to improve the link performance of device-to-device communication using Monte Carlo simulations. In the work [39], a dual-hop hybrid RF and UWOC relay-based communication system is proposed and investigated using nakagami-m fading and Gamma-Gamma distribution. In [40], the outage performance of serial and parallel relay-based UWOC systems is analyzed using a new aggregated fading model for underwater environments. The authors developed a model of an OFDM serial relay UWOC system that works over the combined generalized gamma distribution channel in [41]. To overcome the short-range communication of UWOC, the utilization of autonomous underwater vehicles (AUVs) swarms is proposed and investigated analytically to transmit real-time video

TABLE 1. Summary of literature on Relay-based UWOC.

Literature	Data-rate	Theoretical Analysis/ Experiment	Source	Transmission Range	Relay / Direct	Power Consumption	Complexity	Diversity Gain
[37]	3 bps	Theoretical analysis	LED/laser	few 100 m	Relay-based	High	High	✖
[38]	100 bps	Theoretical analysis	Acoustic	$>$ 300km	Relay-based	High	High	✖
[39]	$<$ 500 kbps	Theoretical analysis	Laser and RF	$<$ 100m	Relay-based	High	High	✖
[40]	1 Gbps	Theoretical analysis	Laser	40 m	Relay-based	High	High	✖
[41]	1.2 Gbps	Theoretical analysis	Laser	100 m	Relay-based	High	High	✖
[42]	few Mbps	Theoretical analysis	LED	few 100 m	Relay-based	Low	High	✖
[31]	1 Gbps	Theoretical analysis	LED/laser /Acoustic	100 m	Relay-based	High	High	✖
Proposed work	0.5 Mbps	Theoretical analysis and Experimental	LED	up to 10 m	Relay-based	Low	Low	✔

streaming in [42]. In [31], numerical simulations have been performed and analyzed to investigate the performance of sector-based opportunistic routing protocols on multi-modal hybrid acoustic and optical wireless communication networks. Although relay communication promises a viable communication alternative for wide-area networks, non-deterministic and unpredictable underwater environments pose numerous challenges for multi-hop optical communication [32], [33], [34]. All the discussed works primarily focused on the numerical and analytical study of the viability of UWSN using various communication technologies in the presence of the underwater's non-deterministic forces. These studies concluded that system performance decreased due to the misalignment, turbulence, and limitations of communication technologies.

In order to mitigate the negative effects of these problems, a relay-based underwater communication system called Aqua-Sense is suggested, designed (prototype), and tested in an emulated underwater environment in this research. Multiple optical receivers are used to increase the relay's coverage area. The coverage area of the beam can also be increased using extended beam width [35]. Furthermore, this technique can also reduce the effects of misalignment and link interruption caused by underwater disturbances [36]. Although the larger beam width increases the coverage of the signal, it also reduces the effective communication link range. Hence, this problem can be solved using higher transmission power or enhanced light intensity of the beam at a certain point.

Due to the narrow beam width of the optical signal, single-input-single-output (SISO) communication shows conservative performance in underwater environments due to factors such as absorption, scattering, and beam fluctuations [2]. Diversity schemes like majority logic combining (MLC), selection combining (SC), and equal gain combining (EGC) can lessen the effects of these disturbances. Prior research reported that the SC provides lower complexity and cost compared to other techniques [1]. Furthermore, SC, MLC, and EGC achieved better bit error rate (BER) performance as compared to the SISO system [13], [21], [22]. The results in [1], [2] show that the BER performance of the diversity schemes is affected by the transmitter power. The results also show that the SC, MLC, and EGC achieve varying performance at a specific transmit power. As a result of the inconsistent brightness levels caused by the changing distance between links, the threshold that distinguishes high and low pulses changes quickly within a certain range, leading to an increased number of packet errors. To mitigate the effects of these challenges, we proposed, designed, and evaluated an optical relay-based communication system. To enhance the transmission power of the sensor node, a plano-convex lens of larger focal length is utilized. The optical relay is designed by considering the change in beam width (transmit power) and signal intensity with varying distances between the transmitter and receiver.

Furthermore, the availability and capacity of optical wireless can be further improved using an RA-UWOC system [23]. Additionally, diversity gain techniques are employed to improve the performance of the relay. The plano-convex lenses are placed strategically such that the received light signal can have maximum impact on the optical receivers and enhance its intensity in a given area (the effective area of the photo-diode) to increase the effective communication range. A novel algorithm is employed at the relay, which strategically selects the combining scheme according to the packet success rate (PSR) or BER at the given link range or environmental parameters. The algorithm also strategically changes the threshold value (V_t), which represents the distinction between binary 0 and 1. The brief comparison of the related previous works are tabulated in Table 1.

The proposed RA-UWOC system can be a viable candidate for applications such as aquaculture, offshore fish farm monitoring, and other underwater environmental surveillance. The opto-relay is considered a stationary module, whereas the opto-sense is supposed to serve as a

mobile node. The communication between the opto-relay and optical receiver is considered to be a fixed line-of-sight communication for maintaining beam alignment. These prototypes exhibit solid capability for future updates and applications for IoUTs based on small wireless UWSN and small mobile platforms due to their compact size, less complex components, and energy efficient modules.

III. CONTRIBUTIONS

The major contributions of this study are stated as follows:

1) We propose an underwater environment and subsea habitats monitoring system utilizing relay-based UWOC. The UWSN comprised three fundamental components; opto-sense, opto-relay, and optical receiver. Specifically, the opto-sense can sense the temperature, water pressure, and altitude of the habitat and transmit it to the opto-relay. The opto-relay processes this data and transmits it to the optical receiver, that forwards this information to the gateway for real-time monitoring of the received information.
2) The opto-relay is powered by combining techniques for diversity gain. The software-based combining techniques, e.g., MLC, EGC, and SC, were coded and installed on the microcontroller to achieve superior performance.
3) The prototype opto-sense and opto-relay were designed and fabricated. The fabricated system was evaluated in a water tank of 4 meters to verify its feasibility, reliability, and practicality. The system was evaluated by exposing it to a variety of major disturbances (induced by the effects of absorption and scattering) that can impact its communication efficiency. In particular, the water turbulence was emulated using two powerful water motor jets. A population of small air bubbles was generated using a two-outlet aerating jet. The turbidity level of water was varied by mixing a zinc oxide solution in water.
4) The nondeterministic nature of the underwater environment and the varying beam width of the optical signal with distance create a considerable amount of error and ultimately corrupt the transmitted data. To mitigate these challenges, a channel-aware algorithm was proposed and installed for switching various combining techniques according to the in-situ packet success rate or bit error rate.
5) The proposed UWOC system was theoretically evaluated with the assistance of experimental data to compare the bit error rate (BER) performance of the combining techniques with and without relay.

The subsequent sections of the paper adhere to the following structure: Section IV comprehensively examines the implementation of hardware and software components. In Section V, a thorough theoretical analysis of the proposed relay system with diversity gain is presented. Section VI is dedicated to the discussion of experimental and theoretical evaluations, as well as the corresponding results. Finally, Section VII succinctly summarizes the study's findings and conclusions.

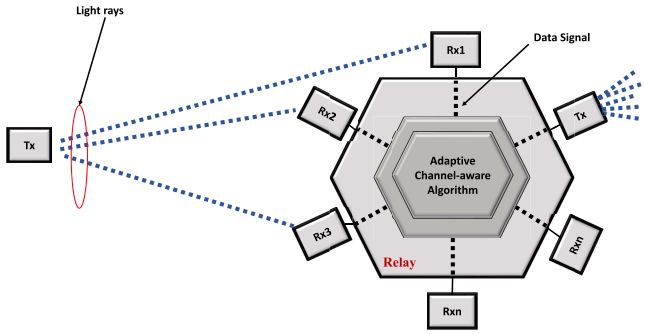

FIGURE 2. The operational mechanism of the proposed relay-based underwater optical wireless communication (UWOC) system.

IV. METHODOLOGY AND COMPONENTS

The proposed RA-UWOC system is composed of underwater sensor nodes (opto-sense), an optical relay (opto-relay), and an optical receiver. The opto-sense senses the underwater environment using a variety of sensors, transforms the information into digital bits, and transmits the packets to the opto-relay via the UWOC system. The opto-relay captures these streams of optical signals by using numerous closely positioned optical receivers. The number of receivers capable of accurately decoding the received signal with minimal errors is determined by the effective beam width/area of the optical signal that is incident on the opto-relay. Therefore, the signal's reception by each optical receiver is determined by the proximity of the opto-sense to the opto-relay. Before receiving each payload packet, the opto-relay assesses the PSR/BER performance of each combining technique (CT) and chooses the most optimum CT to receive the payload. Afterward, the opto-relay transfers the payload to the optical receiver located at the final gateway. The operational mechanism of this process is illustrated in Figure 2. The major components of the RA-UWOC system are briefly discussed in the following subsections.

A. UNDERWATER WIRELESS SENSOR NODE

The opto-sense comprises a depth sensor (MS5837-02BA, Blue-Robotics, USA), an optical transmitter, and a collimated lens to align and focus the optical beam in a given direction. This depth sensor can measure an absolute pressure up to 2 bar (10 m depth) with a depth resolution of 0.16 mm and an in-air altitude resolution of 13 cm. The ultrahigh-resolution depth sensor was bridged with the microcontroller (nRF52840, Nordic Semiconductor, Norway) using the I^2C interface. The block diagram and the pictorial presentation of the sensor node are illustrated in Figure 3. The bar02 sensor recorded the temperature, water pressure, and altitude of the habitat and transmitted the data to the microcontroller (MCU), which converted the data to digital signals for

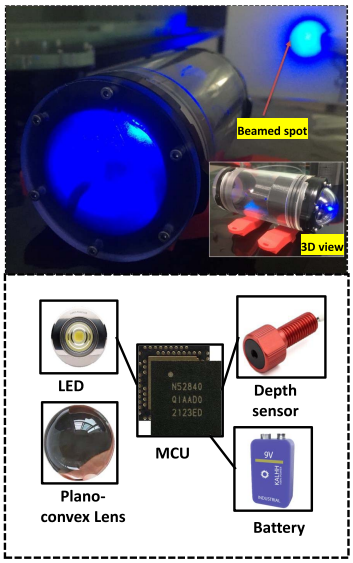

FIGURE 3. Building blocks of the prototype opto-sense node.

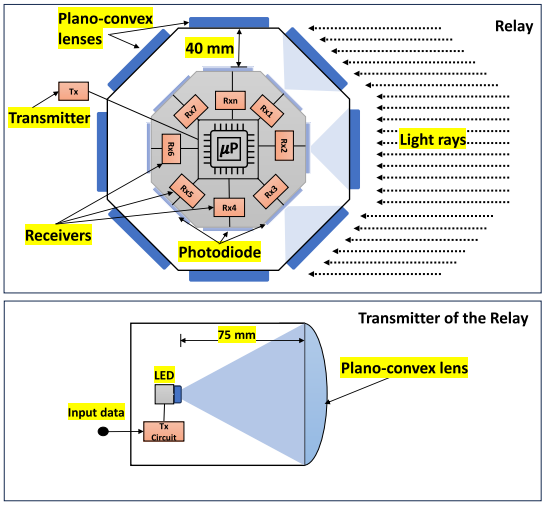

FIGURE 4. Design parameters of optical relay.

driving the optical signal. The driver circuit was used to modulate the optical signal across the channel [12]. An LED (wavelength: 470 nm; G05BC09, Hyper Flux 5pie, China) and planoconvex lens (focal length: 40 mm; LA1304-AB, Thorlabs, USA) were utilized as an optical source and collimated lens, respectively. The combined modules were fitted in a water-tight enclosure (Blue Robotics, USA), which can withstand a depth of up to 60 m. The opto-sense was powered with a 7.4 V compact Li-po battery (21E03, BLL, China) to provide improved mobility and compactness. The fabricated prototype opto-sense is depicted in Figure 3.

B. OPTO-RELAY

The optical relay contained multiple optical receivers to increase the efficiency, performance, and mitigation of the bit errors. We used photo-detectors (S5107, Hamamatsu, Japan) based on the avalanche photo-diode (APD) to detect the optical signal originating from the opto-sense. The individual optical receiver is composed of a photodetector, a planoconvex lens, and a transimpedance-based efficient receiver circuit. The 48 MHz MCU (nRF52840, Nordic Semiconductor, Norway) was applied to recognize the incoming electrical signal and convert it into a realizable digital stream. An optical receiver incorporating a trans-impedance amplifier (TIA) as described in Section IV-C was employed to convert the optical signal into a continuous digital electrical signal [12]. Furthermore, a planoconvex lens with a focal length of 40 mm from Thorlab was used to hone the incoming optical signal onto the compact photodetector. The photo-detectors were positioned at a distance of around 40 mm from the corresponding planoconvex lens in order to maximize the intensity of the optical signal on the $15 \times 17mm^2$ reception area of the photodetector. When the optical signal is directed towards the opto-relay, the M number of photo-detectors (PDs) detects this optical signal and transforms it into a measurable voltage, continuously. The resultant signal consists of consecutive pulses of high and low voltages. The TIA-based optical receiver of each receiver module transforms this signal into a rectangular pulse train with less attenuation and electrical noise. This smoother incoming signal is passed to the MCU for signal processing. The physical configurations of the opto-relay prototype considering the PDs and planoconvex lenses are illustrated in Figure 4. Moreover, a simple software-based intensity modulation/direct detection (IM/DD) was implemented and installed on the MCU to reduce the circuit and processing complexity, which was critical for power-sensitive, affordable applications such as RA-UWSNs and SMP applications. The optical transmitter of the opto-relay comprised a comparator-based driver circuit [12], an optical source (G05BC09, Hyper Flux 5pie, China) of wavelength $\lambda = 470nm$ and a planoconvex lens (LA1608-AB-N-BK7, Thorlabs, USA) of focal length $75mm$. To overcome the size constraint of the opto-relay, a planoconvex lens with an extended focal length was incorporated to amplify the signal and increase the range of communication. The MCU decoded the information and employed an optical transmitter to transmit and redirect the signal. The optical detector at the receiving end was able to detect the signal as it travelled through the water channel. The entire module of the opto-relay was fitted into a transparent acrylic watertight enclosure (BlueRobotics, USA) of 6 inches (15.24 cm) in diameter, which can withstand a depth of up to 65 m. Subsequently, software-based combining techniques such as EGC, MLC, and SC were implemented and installed on the MCU for diversity gain. The combining techniques were deployed by using the voltage intensity of a single pulse (attained by the photodiodes) along with other useful Boolean operations. A brief discussion of these implemented techniques is explored in Section V. The lateral process of these combining techniques, i.e., EGC, MLC, and SC, is illustrated in Figure 5.

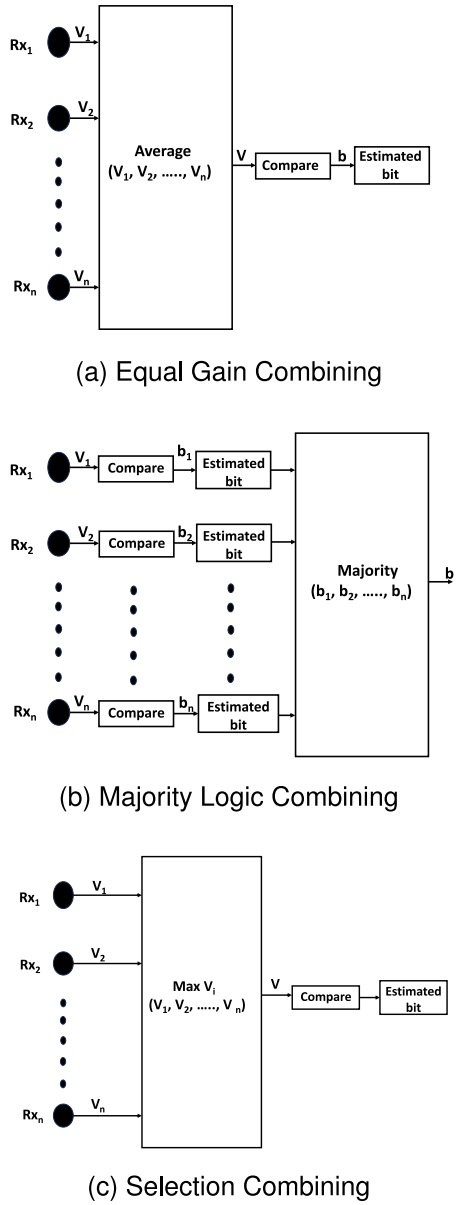

FIGURE 5. Diversity techniques used in proposed UWOC system.

In this context, V denotes the converted voltage derived from the received optical signal, while b represents the estimated bit. The comparison section demonstrates the procedure in which the voltage values $(V_1, V_2, \ldots, V_n)$ are compared to the threshold voltage in order to determine the received bit, either 1 or 0. A comprehensive pictorial presentation of the fabricated opto-relay prototype is illustrated in Figure 6.

C. TRANS-IMPEDANCE AMPLIFIER (TIA)-BASED OPTICAL-RECEIVER

The receiver circuit [12] consists of a buffer (TL082), amplifier (TL082), comparator (LM393), and −5V generator (LMC7660). The voltage-follower buffer component collects a constant and weak opto-to-electric signal. The TL082 amplifier then amplifies this signal, increasing its strength by up to 100 times. The amplified signal is then sent to the LM393 for a transistor-transistor logic (TTL) comparison, where it is compared to either 0 or 5 volts. The LMC7660 integrated circuit (IC) is used for the purpose of producing a negative voltage of −5 V, in order to facilitate the tasks of buffering and amplification.

D. PROPOSED EFFICIENT ALGORITHM FOR THE OPTO-RELAY

Owing to the turbulent nature of underwater environments, the channel characteristics of the medium vary constantly within a short period of time [43]. The link for communication between the opto-sense and opto-relay is very unstable and needs to be constantly adjusted. This is especially true if the opto-sense is deployed on a moving object, like a marine habitat. Therefore, the sensitivity threshold of the optical receivers should adapt to the surrounding environment and channel characteristics. To mitigate the effects of this challenge, an adaptive channel-aware algorithm is proposed, designed, and evaluated in this study.

The algorithm consists of two modules: Optimum CT Selection (OCS) and Reception Performance Status (RPS). Both modules operate sequentially on the opto-relay. The algorithm operates in two modes: the first mode calculates the minimal bit error rate (MinBER) and the corresponding average voltage gain (AVG) value after each combining technique is executed consecutively (estimation mode). The second mode of the algorithm involves the reception of the payload packets (reception mode).

The algorithm executes in three time slots: estimation time, payload reception time, and payload forward time. Initially, during the estimation period, the opto-sense transmits five packets (each containing 8 bits, including the header byte, synchronization byte, channel estimation packet, payload, and end byte) to the opto-relay.

The opto-relay receives the estimation packet (0× FF) via multiple optical receivers. Initially, the photo-diode specifications determine the default threshold voltage (V_t) to a specific value. The high bits (1's) of the channel estimation packet translate to maximum voltage gain at the opto-relay. The voltage gain of the individual optical receiver is contingent upon its proximity to the centre of the optical signal's beam spot. Initially, the infinite machine calls the OCS algorithm by updating the value of token (T) as "HIGH" to obtain the MinBER and AVG values, which translate to binary 1 in machine language. The token is used to specify the mode of the algorithm.

The opto-relay receives the high pulse of the combining technique estimator packet (CTE) consecutively and converts them into corresponding voltages, $RG_1, RG_2, ., RG_n$ (originating from each receiver) and consecutively runs the combining technique functions for each bit. The methodology and building blocks of all the combining techniques are illustrated in Figure 5, considering the multiple arguments

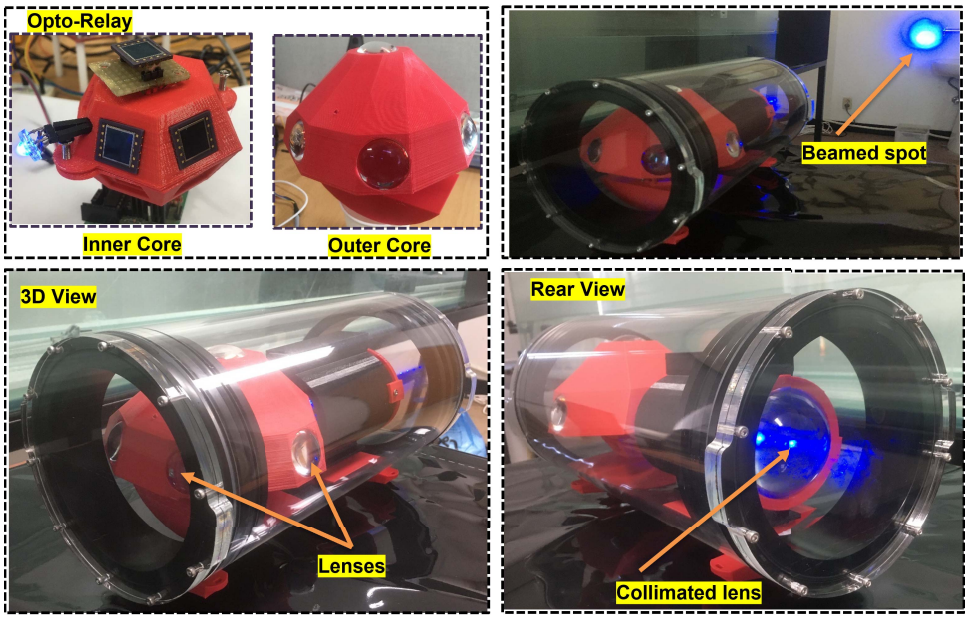

FIGURE 6. Prototype design of opto-relay module.

and return variables:

$$(BER_{EGC}, MV_{EGC}, RP)\textbf{EGC\_func}(i, T, CT_{ID}, RG_1, RG_2, ., RG_n) \quad (1)$$

$$(BER_{MLC}, MV_{MLC}, RP)\textbf{MLC\_func}(i, T, CT_{ID}, RG_1, RG_2, ., RG_n) \quad (2)$$

$$(BER_{SC}, MV_{SC}, RP)\textbf{SC\_func}(i, T, CT_{ID}, RG_1, RG_2, ., RG_n) \quad (3)$$

During the estimation process, these functions, (1), (2), (3), return the respective BER and the mean voltage (MV) after consecutively executing the CTs. The bit-by-bit (i) reception of the CTE utilizing the EGC, MLC, and SC, respectively, yielded the BER and MV values that are represented by the BER_{EGC}, BER_{MLC}, BER_{SC}, MV_{EGC}, MV_{MLC}, and MV_{SC}. The MV value is calculated by dividing the sum of all the voltage gains from the receivers by the total number of receivers. The received payload packet (RP) provides a null value during the estimation mode, but it returns the received payload during the reception mode. During the estimation mode, the CT_{ID} is assigned a null value, but during the reception mode, its value is updated to $MinBER_{ID}$. The CT_{ID} determines the specific CT to be used during the reception mode for receiving the payload packet.

The OCS algorithm uses these BER values, i.e., BER_{EGC}, BER_{MLC}, and BER_{SC}, to select the combining technique with the best BER performance. The OCS algorithm returns the identification key along with the corresponding average voltage gain value (AVG) obtained by the respective best-performing combining technique to the main infinite machine. This identification key, $MinBER_{ID}$, and AVG are used to select the best-performing combining technique, and V_t for the current reception of payload packets.

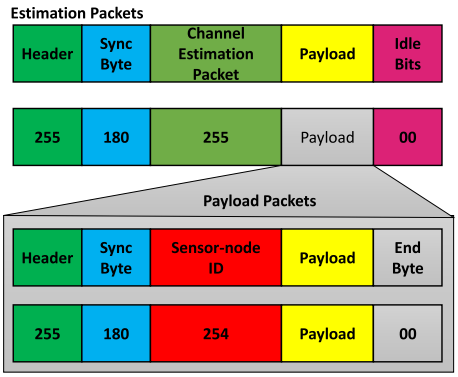

FIGURE 7. Data frame used in transmission.

After the estimation process, the reception mode of the RPS algorithm is activated by enabling the token (T) as "LOW" or binary 0. During this process, the selected combining technique is used, and the RPS receives the payload packets comprising the header byte (0×255 in hexadecimal) to initiate the identification of the payload, synchronization byte (0×180 in hexadecimal), sensor node identification key, sensor data (temperature, pressure, altitude data from the Bar02 sensor), and end byte (0×00 in hexadecimal) for identifying the end of the payload packet. The payload packet has a total size of 7 bytes.

The functions (1), (2), (3) return a null value for both the BER and the MV during the reception mode. The data frame utilized during the transmission is presented in Figure 7. At the final stage, the opto-relay forwarded these payload packets to the stationary optical receiver, which possessed a reliable communication link to the external world for real-time monitoring and tangible analysis. The pseudocodes

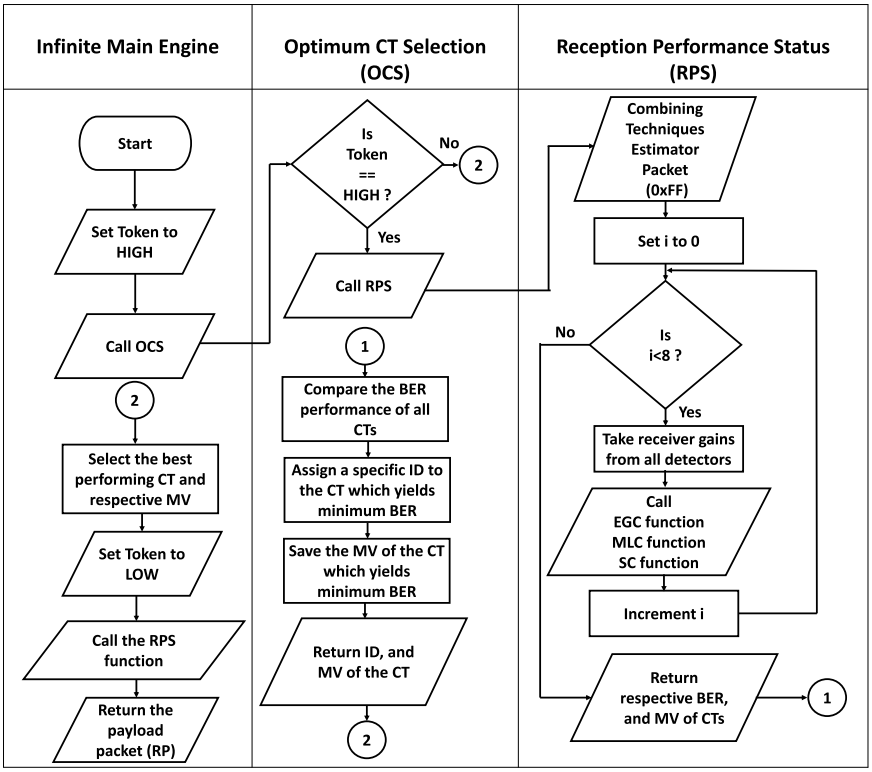

FIGURE 8. Flow chart of channel-aware adaptive algorithm used in proposed relay-based UWOC system.

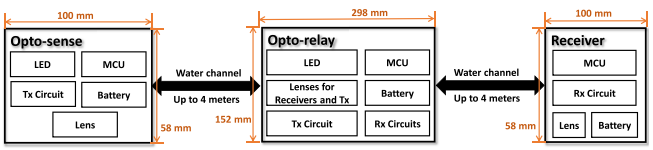

FIGURE 9. Building blocks of the proposed tested system.

of the proposed adaptive algorithms, OCS, and RPS, are illustrated in Algorithms 2 and 1, respectively. The flowchart of the proposed algorithm is depicted in Figure 8.

The Figure 9 depicts the block diagram of the relay-based UWOC system, showcasing its modules together with their subcomponents.

V. SYSTEM MODEL AND PERFORMANCE ANALYSIS

The theoretical BER analysis of the proposed system was evaluated with and without a relay.

A. WITHOUT RELAY

The data received at the detector can be expressed as

$$Y = hs + n, \tag{4}$$

where $s \in \{0, 1\}$ represents the information bits, 'h' denotes the channel fading coefficient or impulse response, and 'n' indicates the additive white Gaussian noise with mean and variance. Herein, we derived the experimental data (received data) for numerical analysis, such as the evaluation of mean and variance. The input data used in the theoretical analysis is obtained by conducting experiments in an artificially induced real environment, as discussed in [12]. Therefore, the data

Algorithm 1: Reception Performance Status, RPS

Input: Combining Techniques Estimator Packet, $CTE = \{0 \times 255\}$, Token, $T = \{High, Low\}$

Output: Bit Error Rate, $BER^* = \{BER_{EGC}, BER_{MLC}, BER_{SC}\}$, Mean Voltage, $MV^* = \{MV_{EGC}, MV_{MLC}, MV_{SC}\}$

Initialization: Receivers Gain, $RG^* = \{RG_1, RG_2, ..., RG_n\}$
$MV \leftarrow \emptyset$; $T \leftarrow \{High\}$; $CT_{ID} \leftarrow \emptyset$

for $i = 0$ to 8 **do**
  Returns the respective BER, and MV from corresponding CT,
  $RG_1 \leftarrow pinvoltage_1$
  $RG_2 \leftarrow pinvoltage_2$
  $RG_3 \leftarrow pinvoltage_3$
  $RG_n \leftarrow pinvoltage_n$
  Call **EGC_func** $(i, T, CT_{ID}, RG_1, RG_2, ., RG_n)$
  Call **MLC_func** $(i, T, CT_{ID}, RG_1, RG_2, ., RG_n)$
  Call **SC_func** $(i, T, CT_{ID}, RG_1, RG_2, ., RG_n)$
end for
return BER^*, MV^*

Algorithm 2: Optimum CT Selection, OCS

Input: Token, $T = \{High, Low\}$
Output: Min Bit Error Rate, $MinBER_{ID}$, Average Voltage Gain, AVG
Initialization:
$MinBER_{ID} \leftarrow \emptyset$; $T \leftarrow \{High\}$; $AVG \leftarrow \emptyset$; $CT_{ID} \leftarrow \emptyset$
Call RPS (T, CTE, CT_{ID})
if $(BER_{EGC} > BER_{MLC}$ and $BER_{EGC} > BER_{SC})$ **then**
  $MinBER_{ID} \leftarrow 3$; $AVG \leftarrow MV_{EGC}$
else if $(BER_{MLC} > BER_{EGC}$ and $BER_{MLC} > BER_{SC})$ **then**
  $MinBER_{ID} \leftarrow 4$; $AVG \leftarrow MV_{MLC}$
else if $(BER_{SC} > BER_{EGC}$ and $BER_{SC} > BER_{MLC})$ **then**
  $MinBER_{ID} \leftarrow 5$; $AVG \leftarrow MV_{SC}$
end if
return $MinBER_{ID}$, AVG

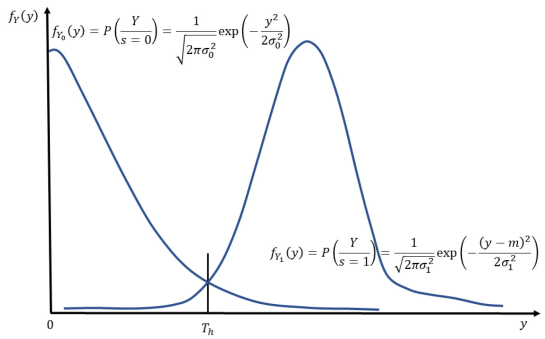

FIGURE 10. Received data for information bits of '0' and '1'.

received at the receiver has already been subjected to various channel impairments, including underwater turbulence, beam attenuation, and pointing errors, which can affect its quality and integrity. Therefore, the set of received data displayed a Gaussian distribution with adequate mean and variance. The sources of the noise included thermal noise, shot noise, and background noise. The data received for '0' were transmitted as

$$f_{Y_0}(y) = P\left(\frac{Y}{s=0}\right) = \frac{1}{\sqrt{2\pi\sigma_0^2}}\exp\left(-\frac{y^2}{2\sigma_0^2}\right), \quad (5)$$

where σ_0^2 denotes the noise variance. Similarly, the data received for '1' were transmitted as

$$f_{Y_1}(y) = P\left(\frac{Y}{s=1}\right) = \frac{1}{\sqrt{2\pi\sigma_1^2}}\exp\left(-\frac{(y-m)^2}{2\sigma_1^2}\right), \quad (6)$$

where m and σ_1^2 represent the mean and variance of the Gaussian distribution function Y, respectively. The data received for the input data '0' and '1' with a threshold T_h are depicted in Figure 10. The variance σ_1^2 represents the optical beam scintillation induced by turbulence.

1) SINGLE INPUT SINGLE OUTPUT (SISO)

In this system, a single beam was used to propagate information and a single detector was used to receive the data. The BER of the proposed system was obtained using

$$P_{siso} = \left(\int_{T_h}^{\infty} P\left(\frac{Y}{s=0}\right)P(s=0)dy + \int_{0}^{T_h} P\left(\frac{Y}{s=1}\right)P(s=1)dy\right), \quad (7)$$

where $P(\cdot)$ represents the probability function.

Integration of the above expression for equiprobable information bits (*i.e.*, $P(S=0) = P(S=1) = 0.5$) is expressed in Eq. (8), where $erf(\cdot)$ denotes the error function, $erf(x) \triangleq \frac{2}{\sqrt{\pi}}\int_0^x e^{-t^2}dt$.

$$P_{siso} = \frac{1}{4}\left(1 - erf\left(\frac{T_h}{\sqrt{2}\sigma_0}\right) + erf\left(\frac{T_h - m}{\sqrt{2}\sigma_1}\right) - erf\left(-\frac{m}{\sqrt{2}\sigma_1}\right)\right) \quad (8)$$

2) SELECTION COMBINING

Among all the irradiances of the detectors, SC obtained the maximum irradiance. The signal obtained at the output of the SC is expressed as

$$Y_{sc} = \max\{Y_1, Y_2, \ldots, Y_M\}, \quad (9)$$

where $Y_1, Y_2, \ldots, Y_M$ denote the irradiance of M detectors. The PDF associated with the maximum irradiance among all the available detectors' irradiance can be obtained as [13],

$$f_{Y_{sc}}(y_{sc}) = M(F_Y(y_{sc}))^{M-1} f_Y(y_{sc}) \quad (10)$$

where $F_Y(y_{sc})$ represents the cumulative distributive function (CDF) of the random variable Y_{sc}. The PDFs obtained using the SC for the information bits "0" and "1" are expressed in Eqs. (11) and (12), shown at the bottom of the next page, respectively. The BER expression derived by substituting Eqs. (11) and (12) in (7) for integration is stated in (13), shown at the bottom of the next page.

$$f_{Y_{sc_0}}(y_{sc}) = P\left(\frac{Y_{sc}}{S=0}\right) = \frac{M}{\sqrt{2\pi\sigma_0^2}}\exp\left(-\frac{y_{sc}^2}{2\sigma_0^2}\right)\left(\frac{1}{2}erf\left(\frac{y_{sc}}{\sqrt{2}\sigma_0}\right)\right)^{M-1} \quad (11)$$

3) MAJORITY LOGIC COMBINING

The majority logic combiner produced the majority of the binary responses via M detectors. The BER expression evaluated using the MLC can be expressed as

$$P_{mlc} = \sum_{i=\lfloor\frac{M+1}{2}\rfloor}^{M}\binom{M}{i}P_e^i(1-P_e)^{M-i}, \quad (14)$$

where $\lfloor\cdot\rfloor$ denotes the floor operator, and P_e represents the BER of SISO as in Eq. (8).

4) EQUAL GAIN COMBINING

The average of the M detector responses was combined to attain a suitable response. The combined response was $Y_{egc} = \sum_{i=1}^{M} \frac{Y_i}{M}$, and the sum of the M independent and identical Gaussian random variables was a Gaussian random variable. Therefore, Y_{egc} denotes a Gaussian random variable with mean 'Mm' and variance '$(M\sigma)^2$'. The density functions for the information bit $s = 0$ or 1 are stated in Eqs. (15) and (16), respectively.

$$f_{Y_{egc_0}}(y_{egc}) = P\left(\frac{Y_{egc}}{s=0}\right) = \frac{1}{\sqrt{2\pi (M\sigma_0)^2}} \exp\left(-\frac{y_{egc}^2}{2(M\sigma_0)^2}\right) \tag{15}$$

$$f_{Y_{egc_1}}(y_{egc}) = P\left(\frac{Y_{egc}}{s=1}\right) = \frac{1}{\sqrt{2\pi (M\sigma_1)^2}} \exp\left(-\frac{(y_{egc} - mM)^2}{2(M\sigma_1)^2}\right) \tag{16}$$

The BER of the equal gain combined system obtained by substituting Eqs. (15) and (16) in (8) and integrating is stated in Eq. (17).

$$P_{egc} = \frac{1}{4}\left(1 - erf\left(\frac{T_h}{\sqrt{2}M\sigma_0}\right) + erf\left(\frac{T_h - Mm}{\sqrt{2}M\sigma_1}\right) - erf\left(-\frac{m}{\sqrt{2}\sigma_1}\right)\right) \tag{17}$$

B. WITH RELAY

The data received at the destination from the source via relay (end-to-end system) is expressed as $Z = hY + n$, where Y denotes the information received at the relay. The CDF of the Z-associated end-to-end relay-based UWOC system can be obtained as follows [47], [48]:

$$F_Z(z) = P(\min\{x, y\} \leq z) = 1 - (1 - F_X(x))(1 - F_Y(y)), \tag{18}$$

where $F_Y(y)$ denotes the CDF of Y from the source to the relay, and $F_X(x)$ represents the CDF of X from the relay to the destination. The BER of the $\mathcal{N}$-hop relay-based end-to-end UWOC system was obtained as follows [49]:

$$P = 1 - \left(1 - P_{e_1}\right)\left(1 - P_{e_2}\right)\cdots\left(1 - P_{e_{\mathcal{N}}}\right), \tag{19}$$

where P_{e_1}, P_{e_2}, and $P_{e_{\mathcal{N}}}$ are BER of the source to first relay, first relay to second relay and $(\mathcal{N}-1)^{th}$ relay to destination for the respective scheme, respectively. Considering uniform channel characteristics from the source to relay as well as the relay to destination (same BER performance, *i.e.*, $P_{e_1} = P_{e_2} = \cdots = P_{e_{\mathcal{N}}} = P_e$), the BER of the end-to-end system is given as [50],

$$P = 1 + \sum_{k=0}^{\mathcal{N}} \binom{\mathcal{N}}{k} (-1)^{\mathcal{N}+1-k} P_e^{\mathcal{N}-k} \tag{20}$$

where P_e is P_{siso}, P_{sc}, P_{mlc}, and P_{egc} for SISO, SC, MLC, and EGC schemes, respectively.

VI. RESULTS AND DISCUSSIONS

The underwater environment is composed of internal forces and random events such as water turbulence, minuscule hanging particles, and small water bubbles. Therefore, the intensity of the optical light decays gradually owing to absorption and scattering, which results in attenuation and random noise [9]. To emulate the real underwater environment for the experiment, a water aquarium equipped with four powerful water pumps and an aerating jet was utilized during the evaluation of the system. The detail analysis and discussion of this setup and the emulation of artificially induced underwater turbulence are explored in our previous research work [12]. The water pump ejected water at a displacement rate of approximately 5 liters per minute, and small air bubbles were created using the aerating jet with an airflow rate of approximately 2.5 liters per minute. The small bubbles were circulated in the water tank using twin tubes laid throughout the tank. Moreover, small holes were drilled in the tubes to randomly place the bubble formation sites. The experiments were conducted in the presence of a light of approximately 100–150 lux, measured at the center of the water tank.

The system was evaluated by calculating the packet success rate, luminous intensity/power at the receiver end, and varying the turbidity level of the water by adding zinc oxide powder. The schematic of the experimental setup is illustrated in Figure 11, and the experimental parameters used in system evaluation are listed in Table 2.

The combining techniques were evaluated using the packet success rate performance of each technique by altering various parameters such as communication link range, data rate, and turbidity level of the water. The efficacy of the combining techniques was assessed by sequentially transmitting 20,000 packets of dummy estimation packets

$$f_{Y_{sc_1}}(y_{sc}) = P\left(\frac{Y_{sc}}{S=1}\right) = \frac{M}{\sqrt{2\pi\sigma_1^2}} \exp\left(-\frac{(y_{sc} - m)^2}{2\sigma_1^2}\right)\left(\frac{1}{2}\left(erf\left(\frac{y_{sc} - m}{\sqrt{2}\sigma_1}\right) - erf\left(-\frac{m}{\sqrt{2}\sigma_1}\right)\right)\right)^{M-1} \tag{12}$$

$$P_{sc} = \frac{1}{2}\left(\int_{T_h}^{\infty} f_{Y_{sc_0}}(y_{sc})dy_{sc} + \int_{0}^{T_h} f_{Y_{sc_1}}(y_{sc})dy_{sc}\right) = \frac{1}{2^{M+1}}\left(1 - \left(erf\left(\frac{T_h}{\sqrt{2}\sigma_0}\right)\right)^M + \left(erf\left(\frac{T_h - m}{\sqrt{2}\sigma_1}\right) + erf\left(\frac{m}{\sqrt{2}\sigma_1}\right)\right)^M\right) \tag{13}$$

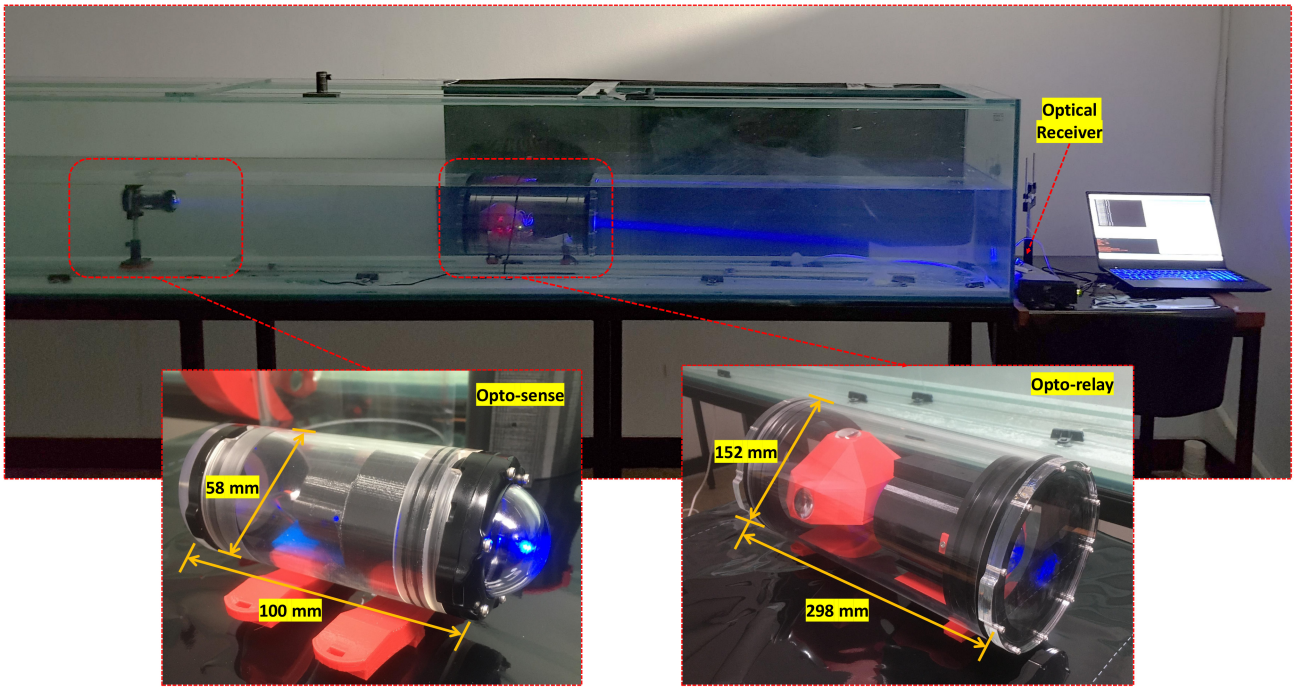

FIGURE 11. Experimental setup.

TABLE 2. Experimental parameters used in system evaluation.

Transmitter	DC Power Battery		5 V
	LED	Power (mW)	102
		Luminous Intensity/power (mcd)	2500
		Luminous Flux (lm)	1.5
		Wavelength (λ)	470
Channel	Aerating Jets	Airflow rate (L/min)	2.5
		No. of outlets	2
	Water Pump (Displacement Rate (L/min))		5
	Lighting Intensity (surroundings) (lux)		100-150
	Turbidity (NTU)		0.01, 25
Receiver	Data Rate (Kbps)		230.4
	SiPIN PD	Photosensitive Area (mm^2)	10x10
		Peak Sensitivity Wavelength (nm)	960

(0×FF) for each combining technique under certain experimental conditions. PSR has been calculated successively for each combining technique at the conclusion of this transmission session. The proposed RA-UWOC was tested against SISO communication (without relay) in water with different levels of turbidity to check the system's viability in highly turbid water. In addition, the theoretical analysis of the proposed system was simulated to obtain the BER results for comparison and further investigation.

A. COMBINING TECHNIQUES PERFORMANCE COMPARISON

For performance evaluation, we calculated the packet success rate at the optical receiver by varying the link distances (up to 4 m), data rate, and turbidity of the water. Moreover, the lux intensity of the optical beam was measured at the opto-relay. During this experiment, the turbidity level of the water was maintained constant at approximately 0.01 NTU. During this experimental evaluation, the opto-sense was placed at a distance of 2 m (link range) from the opto-relay. The packet success rate performance of the system with respect to the varying data rates is illustrated in Figure 12. The measured light intensity at the opto-relay stays steady as the data rate increases. At data speeds of 2.4, 115.2, and 500 kbps, the receiver detected 8.84, 6.27, and 5.3 lux, respectively. The intensity difference between the highest and lowest is about 2 lux, which is insignificant. The system achieved packet success rates of approximately 91%, 89%, and 97% using the combining techniques EGC, MLC, and SC, respectively, at a data rate of 2.4 kbps. Moreover, the system achieved PSRs of approximately 78%, 76%, and 74% by running the system with MLC, EGC, and SC, respectively, at a data rate of 115.2 kbps. Furthermore, the system has achieved PSRs of nearly 73%, 71%, and 69% by consecutively utilizing the combining techniques EGC, MLC, and SC, respectively, at a data rate of 500 kbps. These experimental results demonstrated that the combining techniques MLC and EGC achieved improved performances compared to the SC at a higher data rate.

The PSR performance of the system was also tested by changing the communication link range (link distance) between the opto-sense and opto-relay, as shown in Figure 13. During this experimental evaluation, the turbidity level and the data rate of the system were maintained constant at 0.01 NTU and 230.4 kbps, respectively. The proposed relay-based system had a PSR performance of

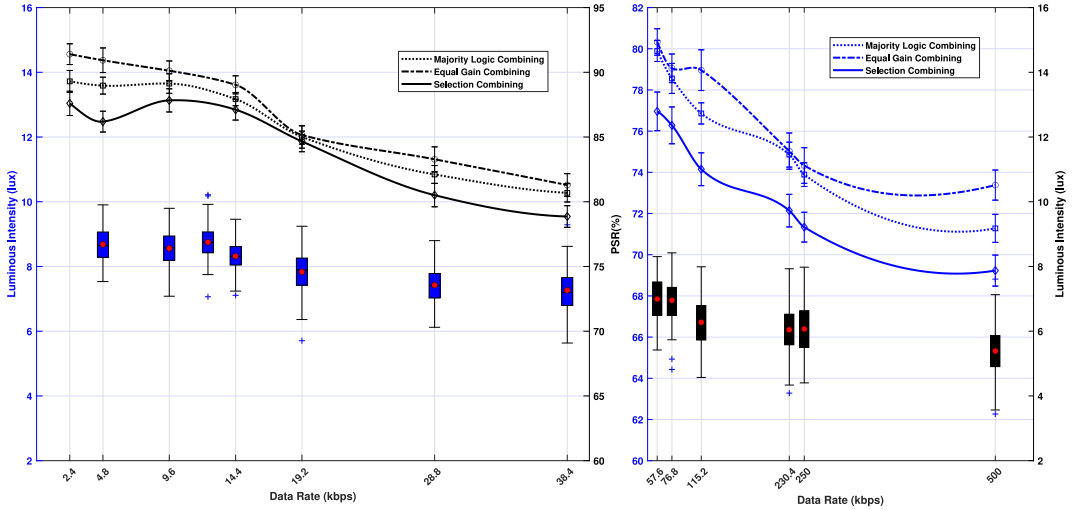

FIGURE 12. Packet success rate performance with respect to varying data rates and signal intensities.

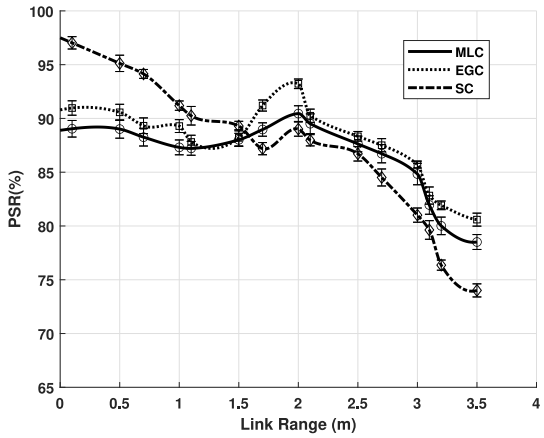

FIGURE 13. Packet success rate performance with respect to communication link range.

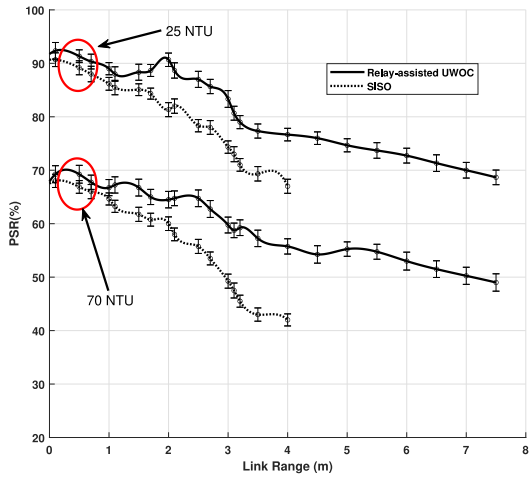

FIGURE 14. Packet success rate performance of relay-assisted UWOC in varying turbidity.

about 97% when the SC combining technique was used, 90% when the EGC combining technique was used, and 89% when the MLC combining technique was used at a link range of 0.1 m. Upon increasing this link range to 2 m, the combining techniques EGC, MLC, and SC achieved PSR performances of approximately 93%, 90%, and 89%, respectively. The system achieved PSR performances of approximately 80%, 78%, and 74% with the combining techniques EGC, MLC, and SC, respectively, at a link range of 3.5 m. These results revealed the enhanced performance of the SC technique for short-range communication of $<$ 1.5 m, whereas the EGC and MLC were more suitable for medium-range communication ($>$ 3 m). Overall, these PSR performances demonstrated the reliability and feasibility of the system for underwater environmental monitoring in aquaculture and other applications.

The relay-assisted UWOC powered by the channel-aware algorithm was evaluated at varying levels of water turbidity. The performance results of this evaluation are presented in Figure 14. The system underwent testing in the presence of very turbid water with turbidity levels of 25 and 70 NTU. Throughout this experimental evaluation, the system's data rate was configured to 0.2 Mbps. The link range is defined as the sum of the distance between the opto-sense and the opto-relay, as well as the distance from the opto-relay to the end receiver. More importantly, the PSR performances displayed promising results in extremely turbid water. The results revealed that the proposed relay-assisted UWOC system and conventional SISO achieved comparable results within the communication link range of approximately 1.5 m in the presence of turbid water of both 25 and 70 NTU. The relay-based UWOC and SISO achieved 68% PSR at a link range of 7.5 m and 67% PSR at 4 m in turbid water at 25 NTU. Nonetheless, the PSR performance degraded exponentially in the presence of extremely turbid water. In the presence of 70 NTU turbid water, the proposed relay-assisted UWOC system achieved only 49% PSR at a link range of 7.5 m,

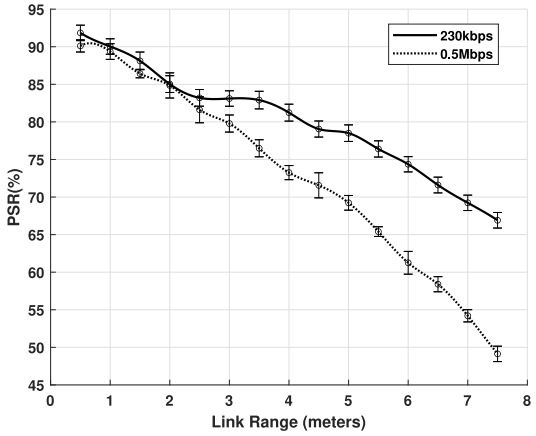

FIGURE 15. PSR performance of the system with varying transmission rate.

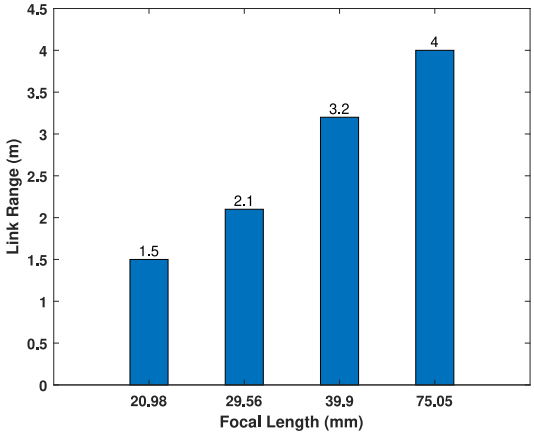

FIGURE 16. Link range of the opto-sense with varying lenses of different focal length.

whereas the SISO achieved 42% PSR at a link range of 4 m. These results confirmed the viability of the proposed system in the presence of water with a turbidity of < 25 NTU.

The Fig. 15 illustrates the system's performance of the opto-sense at transmission rates of 230 kbps and 0.5 Mbps. The figure demonstrates that both systems had similar PSR performance up to a link range of 3 meters. Beyond this range, the performance of the 0.5 Mbps system significantly declined in comparison to the 230-kbps UOWC system. At a distance of 7.5 meters, the PSR performance disparity between the two systems is around 12%. This graph demonstrates that the 230 kbps system is better suited for a compact and efficient underwater optical communication (UWOC) system specifically built for SMP applications.

The system's performance was assessed by employing lenses with varying focal lengths to determine the maximum achievable link-range (from the opto-sense to the opto-relay) of the opto-sense. The obtained result is depicted in Figure 16. In all instances of this experiment, the link range achieved demonstrated a PSR (packet success rate) exceeding 85% in the presence of 0.01 NTU turbid water. The figure illustrates that the plano-convex lens with a focal length of 75 mm achieved a remarkable link range, surpassing 4 meters, while the lens with a focal length of 20.25 mm achieved a relatively shorter link range of only 1.5 meters. These findings indicate that the use of larger lenses can effectively increase the link range. Consequently, a careful balance must be struck between the desired link range and the physical dimensions of the opto-sense.

To evaluate the proposed channel-aware algorithm, the communication link range between the opto-sense and the opto-relay is varied in 25 NTU turbid water. The obtained PSR performance results are compared with the PSR performance of conventional optical wireless communication without the diversity gain. The conventional communication relay, known as SISO, consists of a single transmitter and a receiver. The obtained result is shown in Figure 17. The result shows that the proposed algorithm has improved the PSR performance of the opto-relay by about 10% at every

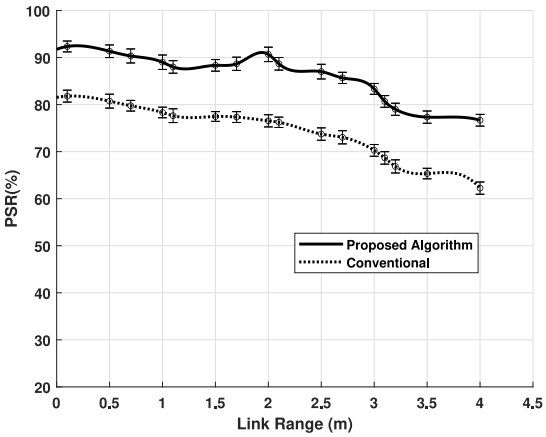

FIGURE 17. Channel-aware algorithm performance.

link range. Due to the divergence in beam width with the increase in distance between the opto-sense and opto-relay, Figure 13 illustrates that the PSR performance of the combining techniques, MLC, EGC, and SC, changes with varying link range. Hence, the proposed algorithm selects the most optimal combining technique for better performance with the respective link range.

To check the validity of this finding, the average run time of each combining technique is calculated at the given link range. The obtained result of this evaluation is shown in Figure 18. To accomplish this, a payload packet containing 20,000 packets of dummy data (0×255) has been sent from the opto-sense to the opto-relay. Subsequently, a counter has been established at the opto-relay to calculate the number of times that the algorithm utilizes each combining technique (EGC, MLC, and SC) to receive packets at various link ranges in the opto-relay. The run-time percentage is determined by dividing the number of times that the algorithm used the particular CT in that link range by the total number of packets, i.e., 20,000. The left axis of the top plot shows the run time percent of combining techniques at the given link range, whereas the right axis illustrates

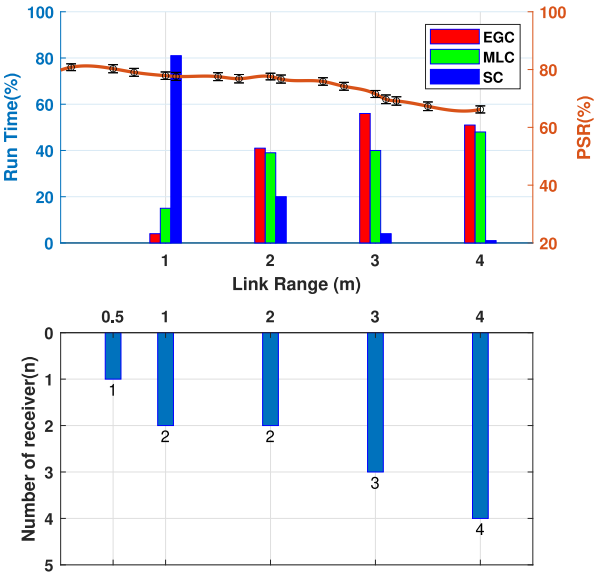

FIGURE 18. Proposed channel-aware algorithm performance (top) run time percentage of respective diversity gain technique (bottom) number of detectors lie inside the beam's cross-section.

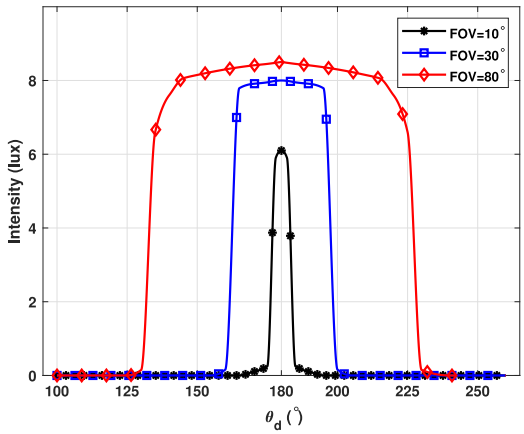

FIGURE 19. Intensity received versus angle of elevation (θ_d) at FOVs of 10°, 30°, and 80°.

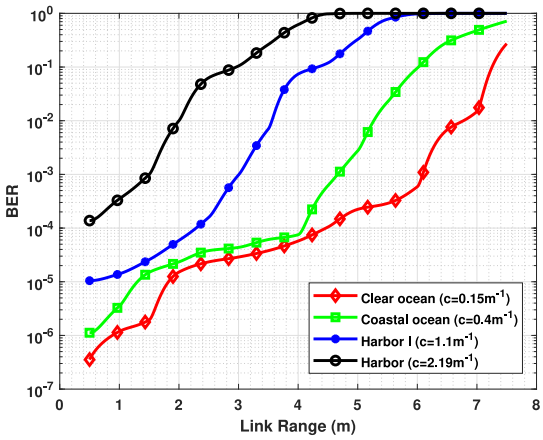

FIGURE 20. BER performance of the Aqua-sense versus link range in different water types.

the PSR performance of the algorithm. This experiment is performed in the presence of moderately turbid water at about 40 NTU. The result shows that the algorithm ran using the combining techniques SC, MLC, and EGC, with an estimated run time of 82%, 15%, and 4%, respectively, at a link range of 1 meter. This finding shows that the SC is more effective for short-distance communication as compared to other techniques. Furthermore, the EGC and MLC have obtained a run time of 51%, and 47%, respectively, at a link range of about 4 meters. This shows that the EGC and MLC are more effective at longer link ranges due to the diverging beam width of the optical signal. However, the PSR performance decreases with varying link ranges. The algorithm has achieved PSR performance of 65%, 64%, 59%, and 51% at the link range of 1 m, 2 m, 3 m, and 4 m, respectively. The bottom plot in Figure 18 illustrates the number of detectors (PDs) that detected the optical signal during these experimental evaluations. The figure shows that the optical signal was detected by 1, 2, 2, 3, and 4 detectors at the link range of 0.5 m, 1 m, 2 m, 3 m, and 4 m, respectively.

Figure 19 illustrates the correlation between the received intensity, the elevation angle of the receiver (θ_d), and the field of view (FOV) of the detector. The figure illustrates that the photodetector gets maximum intensity at the angle θ_d, which is around 180°. The intensity diminishes when the angle θ_d transitions from 180° to 200°, 190° to 200°, and 220° to 230°, with corresponding FOVs of 10°, 30°, and 80°, respectively. The figure also illustrates that the receiver with broader FOVs, namely 30° and 80°, has a larger range window of θ_d, in which the detector may consistently receive greater intensity compared to the detector with a 10° FOV. A possible reason is that a wider FOV allows for more adaptability in varying the θ_d while maintaining a higher intensity level. Expanding the FOV has the potential to enhance system performance by increasing the quantity of photons detected by the detector. These data indicate that the mismatch of the θ_d might cause substantial misalignment, leading to a reduction in received intensity. Additionally, using detectors with a wider field of view can lessen the negative effects of this misalignment.

Figure 20 presents the BER performance of the Aqua-sense in various water types. The figure illustrates the attenuation coefficient (c) for clear ocean water, coastal ocean water, harbor I water, and harbor water. The value of c can be adjusted by adjusting the turbidity level of the water [12]. The Aqua-sense is capable of achieving a BER performance of 1×10^{-2} at link ranges of 6.5 m, 5.2 m, 3.5 m, and 1.9 m in clear ocean water, coastal ocean water, harbor I water, and harbor water, respectively.

B. COMPARATIVE BIT ERROR RATE RESULT

The theoretical and experimental bit error rate (BER) analysis of the proposed system in terms of the link range is depicted in Figure 21. A total of 1×10^7 bits has

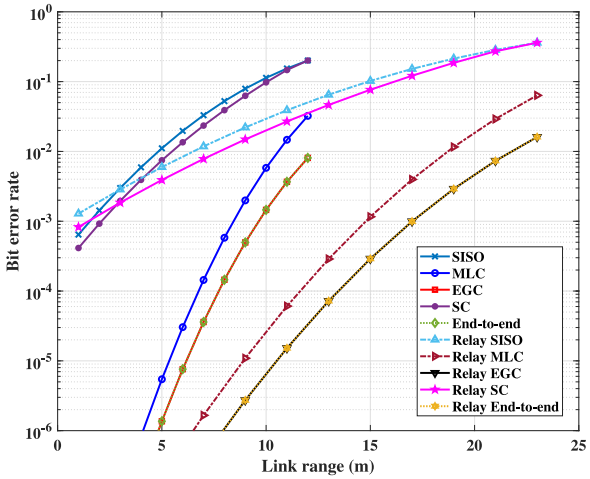

FIGURE 21. Bit error rate of proposed system using with and without relay.

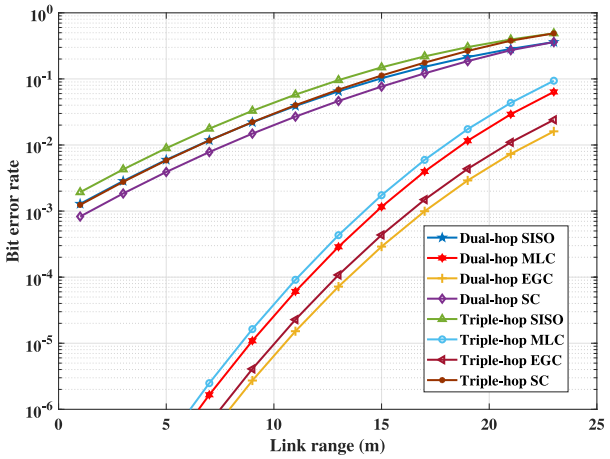

FIGURE 22. Bit error rate performance of dual and triple-hop UWOC system.

TABLE 3. Increase in link range using relay-assisted schemes without relay schemes at 1×10^{-2} BER performance.

Scheme	Link range using Without relay	Link range using With relay	Increase in Link range
SISO	5.00	7.00	2.00
EGC	5.50	7.80	2.30
SC	10.50	18.90	8.40
MLC	12.00	21.50	9.50

been analyzed to determine the BER of 1×10^{-6}. The UWOC system without a relay functioned appropriately up to a link range of 12 *m*, whereas the UWOC system with a relay improved the link range up to 23 *m*. The SISO UWOC system can attain 1×10^{-2} BER performance at a link range of 5 *m*, whereas the relay-assisted SISO UWOC system attained the same BER performance at a link range of 7 *m*. Therefore, using the relay concept, the link range of 2 *m* can be increased at 1×10^{-2} BER performance. The MLC schemes increased the link ranges to 1.5 *m*, 6.5 *m*, and 7 *m* compared with the SC, EGC, and SISO schemes without relays, respectively. However, using the relay-assisted UWOC, the MLC increased the link ranges of 2.6 *m*, 13.7 *m*, and 14.5 *m* over SC, EGC, and SISO schemes, respectively. The theoretical BER results are compared with the BER performance of the respective combining technique in an artificially induced real environment during the experimental process. The theoretical BER results for the relay-assisted SIMO with MLC, EGC, and SC schemes align comparatively with the experimental BER results, as depicted in Figure 21. The depicted figure visually demonstrates the close correspondence between the predicted BER values based on theoretical analysis and the actual BER values obtained through the experimental measurements. The improvements in the link range for the SISO, EGC, SC, and MLC schemes with and without relay at 1×10^{-2} BER performance are listed in Table 3.

The BER performance of the dual-hop (source to relay and relay to destination) and triple-hop (source to first relay, first relay to second relay, and second relay to destination) UWOC system is illustrated in Figure 22. The figure depicts that the dual-hop SISO UWOC system attains 10^{-2} BER at 6.75 *m*, whereas the triple-hop SISO UWOC system attains the same BER performance at 5 *m*. Using the dual-hop UWOC system, the 1.75 *m* link-range can be enhanced when compared with the triple-hop UWOC system at 10^{-2} BER. Similarly, the BER performance gain of the dual-hop over triple-hop UWOC system for the SC, MLC, and EGC schemes is presented in Figure 22.

Figure 23 illustrates the comparison of computational complexity, power efficiency, and spectral efficiency between the OOK modulation technology employed in the system and alternative single-carrier modulation techniques [59]. The y-axis scale depicts a range from low (1) to high (5), with medium being represented by 2.5. Although OOK has low computational complexity, the modulation schemes PAPM, DPPM, and M-PPM generally surpass OOK in terms of power efficiency. The modulation schemes CAP, VPPM, DPPM, and M-PAM exhibit better spectral efficiency in comparison to other schemes. The modulation techniques CAP, PAPM, DPPM, PWM, and OOK have comparable computational complexity. The proposed relay-based underwater optical wireless communication (UWOC) system is specifically tailored for SMP applications, thereby necessitating careful consideration about the size of the sensor node. Consequently, a compromise is made between power efficiency and the level of computational complexity. In addition, reduced computational complexity results in a more straightforward detection method and a less complex receiver circuit. Thus, the OOK modulation has been selected for the relay-based UWOC system owing to its straightforward implementation, minimal circuit complexity, and small physical footprint.

C. MONITORING TERMINAL

For monitoring the Bar02 sensor data, such as temperature, water pressure, and altitude data, we developed a graphical

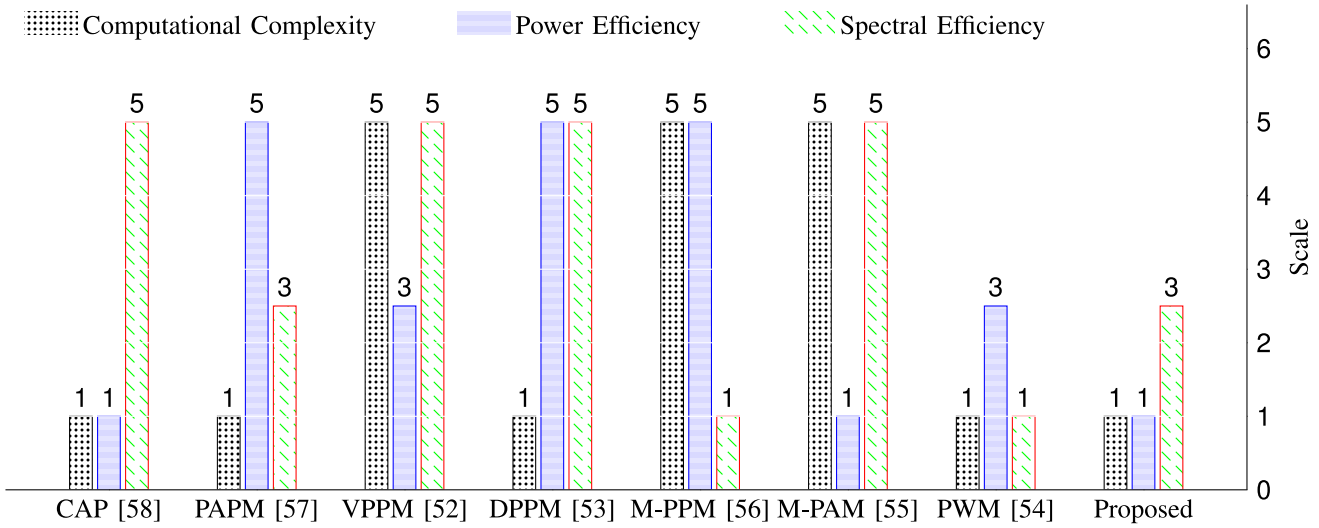

FIGURE 23. Comparative analysis with other works.

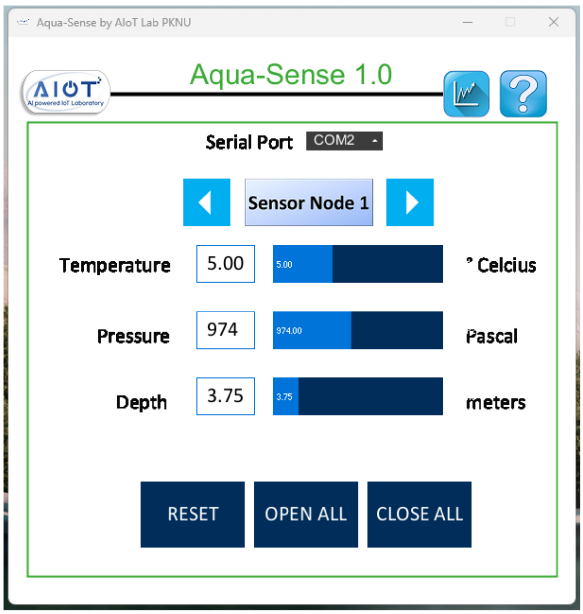

FIGURE 24. Graphical user interface.

TABLE 4. Acronyms and Abbreviations used in paper.

Acronym	Abbreviation
AVG	average voltage gain*
CT	combining technique*
CTE	combining technique estimator packet*
CT_{ID}	combining technique identity*
MinBER	minimal bit error rate*
MV	mean voltage*
NTU	Nephelometric turbidity unit
OCS	optimum CT selection*
PD	photo-diode
PSR	packet success rate
RA-UWOC	relay assisted UWOC
RG	received voltage gain*
RP	received payload packet*
RPS	reception performance status*
SMP	small mobile platform
SISO	single-in-single-out
SIMO	single-in-multiple-out
UWSN	underwater wireless sensor network
V_t	threshold voltage*

user interface (GUI) using the processing software. The GUI comprised an interactive and user-friendly menu organization. To access and monitor the information, the user should select the appropriate serial port (COM) and monitor the instantaneous sensor data emerging from the underwater environment or the subsea habitat. The user can access the past information by clicking the plot button, and this function was enabled by saving the sensor values in a tagged csv file for future access. The pictorial illustration of the GUI is presented in Figure 24.

VII. CONCLUSION

This study proposes a relay-based underwater wireless optical communication system to monitor the diverse information of the underwater environment and subsea habitats. To detect diversity gain, the system was equipped with combining techniques such as EGC, MLC, and SC. The system was evaluated in an emulated underwater environment to review its feasibility, reliability, and efficiency for practical applications. Additionally, an underwater sensor was integrated with the system to monitor the underwater environment. Overall, the experimental evaluations confirmed the viability of the proposed system for IoUT and SMP applications. The present experiments yielded acceptable performance results for a communication link longer than 7 m.

REFERENCES

[1] P. N. Ramavath, S. A. Udupi, and P. Krishnan "High-speed and reliable underwater wireless optical communication system using multiple-input multiple-output and channel coding techniques for IoUT applications," *Opt. Commun.*, vol. 461, Art. no. 125229, Apr. 2020.

[2] M. V. Jamali, J. A. Salehi, and F. Akhoundi, "Performance studies of underwater wireless optical communication systems with spatial diversity: MIMO scheme," *IEEE Trans. Commun.*, vol. 65, no. 3, pp. 1176–1192, Mar. 2017, doi: 10.1109/TCOMM.2016.2642943.

[3] M. A. S. Sejan and W.-Y. Chung, "Lightweight multi-hop VLC using compression and data-dependent multiple pulse modulation," *Opt. Exp.*, vol. 28, no. 13, pp. 19531–19549, 2020.

[4] M. F. Othman and K. Shazali, "Wireless sensor network applications: A study in environment monitoring system," *Procedia Eng.*, vol. 41, pp. 1204–1210, Jan. 2012.

[5] I. Vasilescu, K. Kotay, D. Rus, M. Dunbabin, and P. Corke, "Data collection, storage, and retrieval with an underwater sensor network," in *Proc. 3rd Int. Conf. Embedded Netw. Sensor Syst.*, 2005, pp. 154–165.

[6] C. Detweiller, I. Vasilescu, and D. Rus, "An underwater sensor network with dual communications, sensing, and mobility," in *Proc. Oceans Eur.*, 2007, pp. 1–6.

[7] H. Kaushal and G. Kaddoum, "Underwater optical wireless communication," *IEEE Access*, vol. 4, pp. 1518–1547, 2016.

[8] G. Cossu, "Recent achievements on underwater optical wireless communication," *Chin. Opt. Lett.*, vol. 17, no. 10, 2019, Art. no. 100009.

[9] P. N. Ramavath, A. Kumar, S. Shashikant Godkhindi, and U. S. Acharya, "Experimental studies on the performance of underwater optical communication link with channel coding and interleaving," *CSI Trans. ICT*, vol. 6, no. 1, pp. 65–70, 2018.

[10] R. Santos et al., "Real-time communication support for underwater acoustic sensor networks," *Sensors*, vol. 17, no. 7, p. 1629, 2017.

[11] S. Jiang and S. Georgakopoulos, "Electromagnetic wave propagation into fresh water," *J. Electromagn. Anal. Appl.*, vol. 3, no. 7, p. 5906, 2011.

[12] M. Salman, J. Bolboli, and W.-Y. Chung, "Experimental demonstration and evaluation of BCH-coded UWOC link for power-efficient underwater sensor nodes," *IEEE Access*, vol. 10, pp. 72211–72226, 2022.

[13] P. N. Ramavath, S. A. Udupi, and P. Krishnan, "Experimental demonstration and analysis of underwater wireless optical communication link: Design, BCH coded receiver diversity over the turbid and turbulent seawater channels," *Microw. Opt. Technol. Lett.*, vol. 62, no. 6, pp. 2207–2216, 2020.

[14] M. H. Berlian et al., "Design and implementation of smart environment monitoring and analytics in real-time system framework based on Internet of Underwater Things and big data," in *Proc. Int. Electron. Symp.*, 2016, pp. 403–408.

[15] C.-C. Kao, Y.-S. Lin, G.-D. Wu, and C.-J. Huang, "A comprehensive study on the Internet of Underwater Things: Applications, challenges, and channel models," *Sensors*, vol. 17, no. 7, p. 1477, 2017.

[16] M. Doniec and D. Rus, "Bidirectional optical communication with aquaOptical II," in *Proc. IEEE Int. Conf. Commun. Syst.*, 2010, pp. 390–394.

[17] Y. Tsuchida, N. Hama, and M. Takahata, "An optical telemetry system for underwater recording of electromyogram and neuronal activity from non-tethered crayfish," *J. Neurosci. Methods*, vol. 137, no. 1, pp. 103–109, 2004.

[18] N. Farr et al., "Optical modem technology for seafloor observatories," in *Proc. OCEANS MTS/IEEE*, 2005, pp. 928–934.

[19] N. Saeed, A. Celik, T. Y. Al-Naffouri, and M.-S. Alouini, "Underwater optical wireless communications, networking, and localization: A survey," *Ad Hoc Netw.*, vol. 94, Nov. 2019, Art. no. 101935.

[20] F. Xing, H. Yin, and L. Jing, "Performance characterization of two-way multi-hop underwater networks in turbulent channels," *Chin. Opt. Lett.*, vol. 17, no. 10, 2019, Art. no. 100005.

[21] W. M. Shakir, "Performance analysis of the hybrid MMW RF/FSO transmission system," *Wireless Pers. Commun.*, vol. 109, no. 4, pp. 2199–2211, 2019.

[22] M. K. Simon and M.-S. Alouini, "Digital communications over fading channels (M. K. Simon and M. S. Alouini; 2005) [Book Review]," *IEEE Trans. Inf. Theory*, vol. 54, no. 7, pp. 3369–3370, Jul. 2008.

[23] A. Raza and S. S. Muhammad, "Achievable capacity region of a Gaussian optical wireless relay channel," *J. Opt. Commun. Netw.*, vol. 7, no. 2, pp. 83–95, 2015.

[24] A. Al-Halafi, H. M. Oubei, B. S. Ooi, and B. Shihada, "Real-time video transmission over different underwater wireless optical channels using a directly modulated 520 nm laser diode," *J. Opt. Commun. Netw.*, vol. 9, no. 10, pp. 826–832, 2017.

[25] A. Al-Halafi and B. Shihada, "UHD video transmission over bidirectional underwater wireless optical communication," *IEEE Photon. J.*, vol. 10, no. 2, pp. 1–14, Apr. 2018.

[26] Y. Shao, R. Deng, J. He, K. Wu, and L.-K. Chen, "Real-time 2.2-Gb/s water-air OFDM-OWC system with low-complexity transmitter-side DSP," *J. Lightw. Technol.*, vol. 38, no. 20, pp. 5668–5675, 2020.

[27] S. Han, Y. Noh, U. Lee, and M. Gerla, "Optical-acoustic hybrid network toward real-time video streaming for mobile underwater sensors," *Ad Hoc Netw.*, vol. 83, pp. 1–7, Feb. 2019.

[28] Z. Wang, Z. Lou, X. Xu, Z. Wei, G. Wei, and H. Fu, "Flexible organic photodetector for real-time underwater optical wireless video transmission," in *Proc. Opto-Electron. Commun. Conf. (OECC)*, 2021, pp. 1–3.

[29] B. Priyalakshmi and K. Mahalakshmi, "Performance analysis of video transmission in vertical-UWOC link in mid-sea oil rig IoT systems," *J. Ambient Intell. Hum. Comput.*, vol. 12, pp. 5599–5608, May 2021.

[30] X. Li, X. Hu, R. Zhang, and L. Yang, "Routing protocol design for underwater optical wireless sensor networks: A multiagent reinforcement learning approach," *IEEE Internet Things J.*, vol. 7, no. 10, pp. 9805–9818, Oct. 2020.

[31] A. Celik, N. Saeed, B. Shihada, T. Y. Al-Naffouri, and M.-S. Alouini, "Opportunistic routing for opto-acoustic Internet of Underwater Things," *IEEE Internet Things J.*, vol. 9, no. 3, pp. 2165–2179, Feb. 2021.

[32] Z. Zeng, S. Fu, H. Zhang, Y. Dong, and J. Cheng, "A survey of underwater optical wireless communications," *IEEE Commun. Surveys Tuts.*, vol. 19, no. 1, pp. 204–238, 1st Quart., 2016.

[33] Y. Inoue, T. Kodama, and T. Kimura, "Global optimization of relay placement for seafloor optical wireless networks," *IEEE Trans. Wireless Commun.*, vol. 20, no. 3, pp. 1801–1815, Mar. 2021.

[34] M. Le-Tran and S. Kim, "Performance analysis of multi-hop underwater wireless optical communication systems over exponential-generalized gamma turbulence channels," *IEEE Trans. Veh. Technol.*, vol. 71, no. 6, pp. 6214–6227, Jun. 2022.

[35] A. Celik, N. Saeed, B. Shihada, T. Y. Al-Naffouri, and M.-S. Alouini, "End-to-end performance analysis of underwater optical wireless relaying and routing techniques under location uncertainty," *IEEE Trans. Wireless Commun.*, vol. 19, no. 2, pp. 1167–1181, Feb. 2020.

[36] V. V. Mai and H. Kim, "Adaptive beam control techniques for airborne free-space optical communication systems," *Appl. Opt.*, vol. 57, no. 26, pp. 7462–7471, 2018.

[37] A. Bhowal and R. S. Kshetrimayum, "Performance analysis of one-and two-way relays for underwater optical wireless communications," *OSA Contin.*, vol. 1, no. 4, pp. 1400–1413, 2018.

[38] J. Xu, M. A. Kishk, Q. Zhang, and M.-S. Alouini, "Three-hop underwater wireless communications: A novel relay deployment technique," *IEEE Internet Things J.*, vol. 10, no. 15, pp. 13354–13369, Aug. 2023.

[39] M. Furqan et al., "Selection relay-based RF-VLC underwater communication system," in *Proc. Mach. Learn., Deep Learn. Comput. Intell. Wireless Commun.*, 2020, pp. 177–192.

[40] Y. Jiang, Y. Li, X. Zhang, M. Ju, and P. Huang, "Outage performance analysis for relay-assisted UWOC systems over GGD weak turbulence with nonzero boresight pointing errors," *Phys. Commun.*, vol. 58, Jun. 2023, Art. no. 102017.

[41] Y. Nie, W. Pang, S. Li, P. Wang, and T. Zhang, "Performance investigation of ofdm-based serial relay uwoc system over the generalized gamma distribution," in *Proc. Asia Commun. Photon. Conf. (ACP)*, 2022, pp. 1862–1867.

[42] H. Luo, X. Wang, F. Bu, Y. Yang, R. Ruby, and K. Wu, "Underwater real-time video transmission via wireless optical channels with swarms of AUVs," *IEEE Trans. Veh. Technol.*, vol. 72, no. 11, pp. 14688–14703, Nov. 2023.

[43] Y. Ata, J. Yao, and O. Korotkova, "BER variation of an optical wireless communication system in underwater turbulent medium with any temperature and salinity concentration," *Opt. Commun.*, vol. 485, Apr. 2021, Art. no. 126751.
[44] K. P. Peppas, A. C. Boucouvalas, and Z. Ghassemloy, "Performance of underwater optical wireless communication with multi-pulse pulse-position modulation receivers and spatial diversity," *IET Optoelectron.*, vol. 11, no. 5, pp. 180–185, 2017.
[45] Y. Ata and Y. Baykal, "Scintillations of optical plane and spherical waves in underwater turbulence," *J. Opt. Soc. Amer. A*, vol. 31, no. 7, pp. 1552–1556, 2014.
[46] O. Korotkova, N. Farwell, and E. Shchepakina, "Light scintillation in oceanic turbulence," *Waves Random Complex Media*, vol. 22, no. 2, pp. 260–266, 2012.
[47] N. I. Miridakis, M. Matthaiou, and G. K. Karagiannidis, "Multiuser relaying over mixed RF/FSO links," *IEEE Trans. Commun.*, vol. 62, no. 5, pp. 1634–1645, 2014.
[48] B. K. Levidala, P. N. Ramavath, and P. Krishnan, "High-speed long-range multihop underwater wireless optical communication convergent with free-space optical system for optical Internet of Underwater Things and underwater optical wireless sensor network applications," *Opt. Eng.*, vol. 61, no. 7, 2022, Art. no. 076107.
[49] L. B. Kumar, R. P. Naik, P. Krishnan, A. A. B. Raj, A. K. Majumdar, and W.-Y. Chung, "RIS assisted triple-hop RF-FSO convergent with UWOC system," *IEEE Access*, vol. 10, pp. 66564–66575, 2022.
[50] K. L. Bhargava, P. N. Ramavath, and P. Krishnan, "Performance analysis of multi-hop FSO convergent with UWOC system for security and tracking in navy applications," *Opt. Quant. Electron.*, vol. 54, no. 6, p. 327, 2022.
[51] J. Bolboli, M. Salman, R. P. Naik, and W.-Y. Chung, "Experimental and simulation study of a LoRaWAN-assisted relay for IoUT communication," *IEEE Trans. Green Commun. Netw.*, vol. 8, no. 1, pp. 453–467, Mar. 2024, doi: 10.1109/TGCN.2023.3324638.
[52] F. Delgado, I. Quintana, J. Rufo, J. A. Rabadan, C. Quintana, and R. Perez-Jimenez, "Design and implementation of an Ethernet-VLC interface for broadcast transmissions," *IEEE Commun. Lett.*, vol. 14, no. 12, pp. 1089–1091, Dec. 2010.
[53] D.-S. Shiu and J. M. Kahn, "Differential pulse-position modulation for power-efficient optical communication," *IEEE Trans. Commun.*, vol. 47, no. 8, pp. 1201–1210, Aug. 1999.
[54] V. Guerra, C. Suarez-Rodriguez, O. El-Asmar, J. Rabadan, and R. Perez-Jimenez, "Pulse width modulated optical OFDM," in *Proc. IEEE Int. Conf. Commun. Workshop (ICCW)*, 2015, pp. 1333–1337.
[55] S. Randel, F. Breyer, S. C. J. Lee, and J. W. Walewski, "Advanced modulation schemes for short-range optical communications," *IEEE J. Sel. Topics Quantum Electron.*, vol. 16, no. 5, pp. 1280–1289, Sep./Oct. 2010.
[56] A. Pradana, N. Ahmadi, T. Adiono, W. A. Cahyadi, and Y.-H. Chung, "VLC physical layer design based on pulse position modulation (PPM) for stable illumination," in *Proc. Int. Symp. Intell. Signal Process. Commun. Syst. (ISPACS)*, 2015, pp. 368–373.
[57] Y. Zeng, R. Green, and M. Leeson, "Multiple pulse amplitude and position modulation for the optical wireless channel," in *Proc. 10th Anniv. Int. Conf. Transp. Opt. Netw.*, 2008, pp. 193–196.
[58] P. A. Haigh et al., "Multi-band carrier-less amplitude and phase modulation for bandlimited visible light communications systems," *IEEE Wireless Commun.*, vol. 22, no. 2, pp. 46–53, Apr. 2015.
[59] S. Kumar and P. Singh, "A comprehensive survey of visible light communication: Potential and challenges," *Wireless Pers. Commun.*, vol. 109, pp. 1357–1375, May 2019, doi: 10.1007/s11277-019-06616-3.

MAAZ SALMAN received the M.S. degree in electrical communication system engineering from Soonchunhyang University, Asan, South Korea. He is currently pursuing the Ph.D. degree in artificial intelligence and convergence with Pukyong National University, South Korea. His research areas include AI-assisted IoT, UIoT, underwater sensor network, underwater optical wireless communication, design of passive microwave components, DGS circuit applications and design, and simulation of RF front end components at microwave and radio spectrum.

JAVAD BOLBOLI received the M.Sc. degree from the Amirkabir University of Technology, Tehran, Iran. He is currently pursuing the Ph.D. degree with the Department of Artificial Intelligence Convergence, Pukyong National University, Busan, South Korea. His current research interests include IoT, IoUT, low-power wide-area networks, and optical wireless communication.

RAMAVATH PRASAD NAIK (Member, IEEE) received the M.Tech. degree from the Department of Electronics and Communication Engineering, Motilal Nehru National Institute of Technology, Allahabad, in 2015, and the Ph.D. degree from the National Institute of Technology Surathkal, Surathkal, in 2021. He is currently working as a Assistant Professor with the National Institute of Technology Rourkela, India. He served as a Research Professor with the Research Institute of Artificial Intelligence Convergence, Pukyong National University, Busan, Republic of Korea, from September 2021 to April 2023. His research interests include free-space and underwater optical wireless communication, theory and application of error control codes, and co-operative communication.

WAN-YOUNG CHUNG (Senior Member, IEEE) received the B.Eng. and master's degrees in electronic engineering from Kyungpook National University, Daegu, South Korea, in 1987 and 1989, respectively, and the Ph.D. degree in sensor engineering from Kyushu University, Fukuoka, Japan, in 1998. From 1999 to 2008, he served as an Associate Professor with Dongseo University, Busan, South Korea. He is currently a Professor with the Department of Electronic Engineering, Pukyong National University, Busan. His research interests include wireless sensor networks, ubiquitous healthcare and automobile applications, smart light-emitting systems with visible light communication, and embedded systems. He is the educational and research Group leader for artificial intelligence convergence, which is supported by the Brain Korea 21 (BK21) Four project.